Geo-Mar Lett (2014) 34:399–417
DOI 10.1007/s00367-014-0373-3

ORIGINAL

New constraints on oceanographic vs. seismic control on submarine landslide initiation: a geotechnical approach off Uruguay and northern Argentina

Fei Ai · Michael Strasser · Benedict Preu · Till J. J. Hanebuth · Sebastian Krastel · Achim Kopf

Received: 3 November 2013 / Accepted: 27 April 2014 / Published online: 10 May 2014

Abstract Submarine landslides are common along the Uruguayan and Argentinean continental margin, but size, type and frequency of events differ significantly between distinct settings. Previous studies have proposed sedimentary and oceanographic processes as factors controlling slope instability, but also episodic earthquakes have been postulated as possible triggers. However, quantitative geotechnical slope stability evaluations for this region and, for that matter, elsewhere in the South Atlantic realm are lacking. This study quantitatively assesses continental slope stability for various scenarios including overpressure and earthquake activity, based on sedimentological and geotechnical analyses on three up to 36 m long cores collected on the Uruguayan slope, characterized by muddy contourite deposits and a locus of landslides (up to 2 km^3), and in a canyon-dominated area on the northern Argentinean slope characterized by sandy contourite deposits. The results of shear and consolidation tests reveal that these distinct lithologies govern different stability conditions and failure modes. The slope sectors are stable under present-day conditions (factor of safety >5), implying that additional triggers would be required to initiate failure. In the canyon area, current-induced oversteepening of weaker sandy contourite deposits would account for frequent, small-scale slope instabilities. By contrast, static vs. seismic slope stability calculations reveal that a peak ground acceleration of at least 2 m/s^2 would be required to cause failure of mechanically stronger muddy contourite deposits. This implies that, also along the western South Atlantic passive margin, submarine landslides on open gentle slopes require episodic large earthquakes as ultimate trigger, as previously postulated for other, northern hemisphere passive margins.

F. Ai · B. Preu · T. J. J. Hanebuth · A. Kopf
MARUM – Center for Marine Environmental Sciences, and Faculty of Geosciences, University of Bremen, Leobener Straße, 28359 Bremen, Germany

M. Strasser (✉)
Geological Institute, ETH Zurich, Sonneggstrasse 5, 8092 Zurich, Switzerland
e-mail: strasser@erdw.ethz.ch

S. Krastel
Institute for Geosciences, Kiel University, 24188 Kiel, Germany

F. Ai
State Key Laboratory of Geomechanics and Geotechnical Engineering, Institute of Rock and Soil Mechanics, Chinese Academy of Sciences, 430071 Wuhan, China

Present Address:
B. Preu
Chevron Upstream Europe, Chevron North Sea Limited, Seafield House, AB15 6XL Aberdeen, UK

Introduction

Submarine mass movements are widespread on submarine slopes and play an important role in transporting sediments across the continental slope to the deep sea. They also pose a potential hazard for seabed infrastructures (see overview in Masson et al. 2006). For most submarine landslides, the exact mechanisms initiating slope instability are often not fully understood. Preconditioning factors include sediment intrinsic mechanical stability (e.g. the existence of mechanically weak layers), and overpressure generated by gas hydrate dissociation or rapid sedimentation of low-permeability fine-grained sediments leading to decreased frictional resistance (e.g. Sultan et al. 2004, 2012; Flemings et al. 2008; Harders et al. 2010). Triggering mechanisms such as dynamic stresses imposed by earthquakes, or rapid changes in slope geometry by undercutting or oversteepening can ultimately initiate slope failure (e.g. Sultan et al. 2004; Leynaud et al. 2009). To advance our knowledge of the relationship between preconditioning factors and trigger mechanisms for submarine

landslide initiation, we require detailed site characterization and submarine slope stability analyses integrating geomorphological, sedimentological and geotechnical data (e.g. Sultan et al. 2004). Yet, in comparison to the many mapped submarine landslides in the oceans worldwide (e.g. Hühnerbach et al. 2004; Urgeles and Camerlenghi 2013), the global dataset of such detailed slope stability case studies remains scarce and is virtually lacking for the South Atlantic, thus hampering our ability to draw holistic conclusions on submarine landslide initiation processes. This study contributes a first detailed geotechnical characterization and submarine slope stability assessment along the passive continental margin in the western South Atlantic and a comparison with settings from the North Atlantic.

The general study area is the continental margin off Uruguay and northern Argentina, which is oceanographically characterized by the Brazil-Malvinas current confluence (BMC) zone (35–38°S) and by localized strong bottom currents related to various water masses (e.g. Preu et al. 2013). Furthermore, the shelf and continental slope are influenced by high fluvial discharge and sediment supply from the Rio de la Plata (Fig. 1). As a result, this has long been recognised as an excellent site to explore interactions between gravitational downslope and contour current-driven alongslope sediment transport, along with their influences on seabed morphology. Mass movements are common in open slope and canyon areas off the Uruguayan and Argentinean margin (e.g. Lonardi and Ewing 1971; Klaus and Ledbetter 1988; Krastel et al. 2011). The present study area comprises three subareas: the northern-slide (NS) and the drift-and-scarp (DS) areas northeast off the Rio de la Plata mouth between 35.7–36.4°S on the Uruguayan slope, and the southern-canyon (SC) area close to the Mar del Plata Canyon between 37.4–37.7°S on the northern Argentinean slope. For the NS and DS areas, Krastel et al. (2011) used geophysical and sedimentological methods to study the morphology produced by mass movements. Henkel et al. (2011) applied geochemical methods on surficial mass transport deposits (MTDs) of the NS area to reconstruct recent (<30 years old) submarine landslide scenarios, and hypothesized that an earthquake which occurred in the vicinity in 1988 was possibly the trigger mechanism. For the SC area, Preu et al. (2012, 2013) used seismic data to explain the evolution of contourite terraces. Bozzano et al. (2011) and Voigt et al. (2013) described sedimentary facies and presented age constraints on sedimentation processes respectively, to reconstruct modes and rates of contourite deposition. These investigations have provided a strong background for further quantitative slope stability analyses.

The present study is based on physical and geotechnical data derived from core samples taken from undisturbed slopes of the NS/DS and SC adjacent to morphological scarps and the canyon head respectively, to simulate slope stability under various conditions. The main objective is to investigate how geomorphological and sedimentological features are linked to geotechnical parameters and how these affect submarine slope stability, both in the general study area and on comparable continental slopes worldwide. Furthermore, the earthquake-trigger hypothesis proposed by Henkel et al. (2011) is quantitatively tested using seismic slope stability analysis, and scenarios for future failures are evaluated.

Regional geological, morphologic and oceanographic settings

The Uruguayan and northern Argentinean margin is a passive margin which formed during the opening of the South Atlantic in the early Cretaceous (e.g. Hinz et al. 1999). The Argentinean margin has been subdivided into four tectonic segments separated by transfer fracture zones (Franke et al. 2007). The greater study area is located in the northernmost segment separated by the Salado transfer zone (Fig. 1a). Present-day tectonic activity is characterized by active subsidence, which resulted in some intraplate seismicity aligned along this transfer zone (Sosa 1998). Recent documented earthquakes occurred in 1849, 1888 and 1988 AD (for locations of epicentres, see Fig. 1a; Sosa 1998). The epicentre and magnitude of the 1988 earthquake is not conclusively defined. The seismological observatory of the University of Brazil reported 36.5°S, 53.5°W ±100 km with a regional magnitude of 3.9, whereas NEIC (National Earthquake Information Center) reported 36.27°S, 52.73°W and a body wave magnitude of 5.2 M_b (Assumpção 1998; Sosa 1998). The latter scenario has been selected for the purposes of the present study, in an effort to evaluate if and how that presumably closer and stronger earthquake affected slope stability.

Based on seabed morphology, the Uruguayan slope comprising the mass movement-dominated NS and DS study areas is distinct from the southern canyon-dominated area (SC) on the northern Argentinean slope: the Uruguayan margin is characterized by a smooth topography and gentle slopes of ~1.5 to 2.5°, typical of margins where deposition prevails over erosion (e.g. Ewing and Lonardi 1971; Krastel et al. 2011). However, in 1,200–2,800 m water depth distinct morphological scarps with heights mostly ranging between 60 and 90 m, but in places exceeding 100 m, cut across the gentle slope (Fig. 1b, c). The scarps are 10–20° steep but the orientation of the 20–40 km long scarps varies from contour-parallel to more complex geometries perpendicular, parallel and oblique to the depth contours in the DS and NS areas respectively (Krastel et al. 2011). Reflection seismic and parametric sub-bottom profiles across these scarps reveal multiple lines of evidence for gravitational slope instabilities and MTDs (Fig. 2a, b). Seaward-dipping discontinuities cut across the stratigraphic succession and appear to be associated with scarps on the seafloor. While the scarps in the NS area are associated with MTDs occurring repeatedly throughout the stratigraphic succession and suggesting translational sliding (Fig. 2a; Krastel et al. 2011), there is no clear indication for

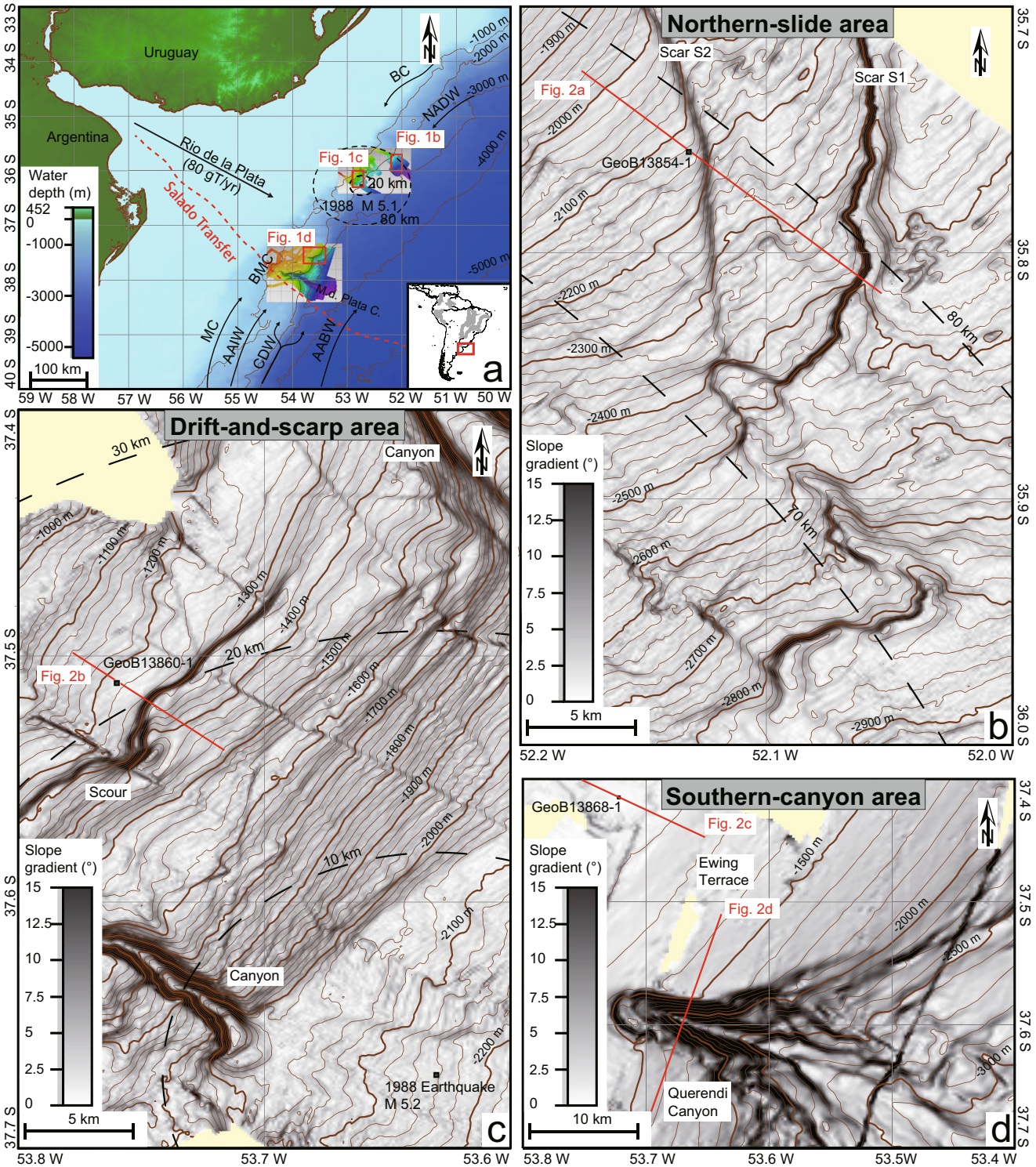

Fig. 1 **a** Map showing the location of the study area and the oceanographic setting along the Uruguayan and northern Argentinean margin (modified after Krastel et al. 2011). *AABW* Antarctic Bottom Water, *AAIW* Antarctic Intermediate Water, *CDW* Circum Polar Deep Water, *NADW* North Atlantic Deep Water, *BMC* Brazil-Malvinas confluence, *BC* Brazil Current, *MC* Malvinas Current, *M. d. Plata C.* Mar del Plata Canyon. *Black dashed lines* Distances to 1988 earthquake epicentre. **b**–**d** Bathymetric and slope gradient maps of the NS (northern-slide, **b**), DS (drift-and-scarp, **c**) and SC (southern-canyon, **d**) areas. *Red lines* Positions of Parasound and seismic profiles shown in Fig. 2, *black squares* core locations

MTDs directly associated with scarp formation in the DS area (Fig. 2b). Rather, the presence of contour-parallel channels and mounded structures at the base of the scarps points to a close interaction between downslope (gravitational) and alongslope (contouritic) sediment transport (Krastel et al. 2011).

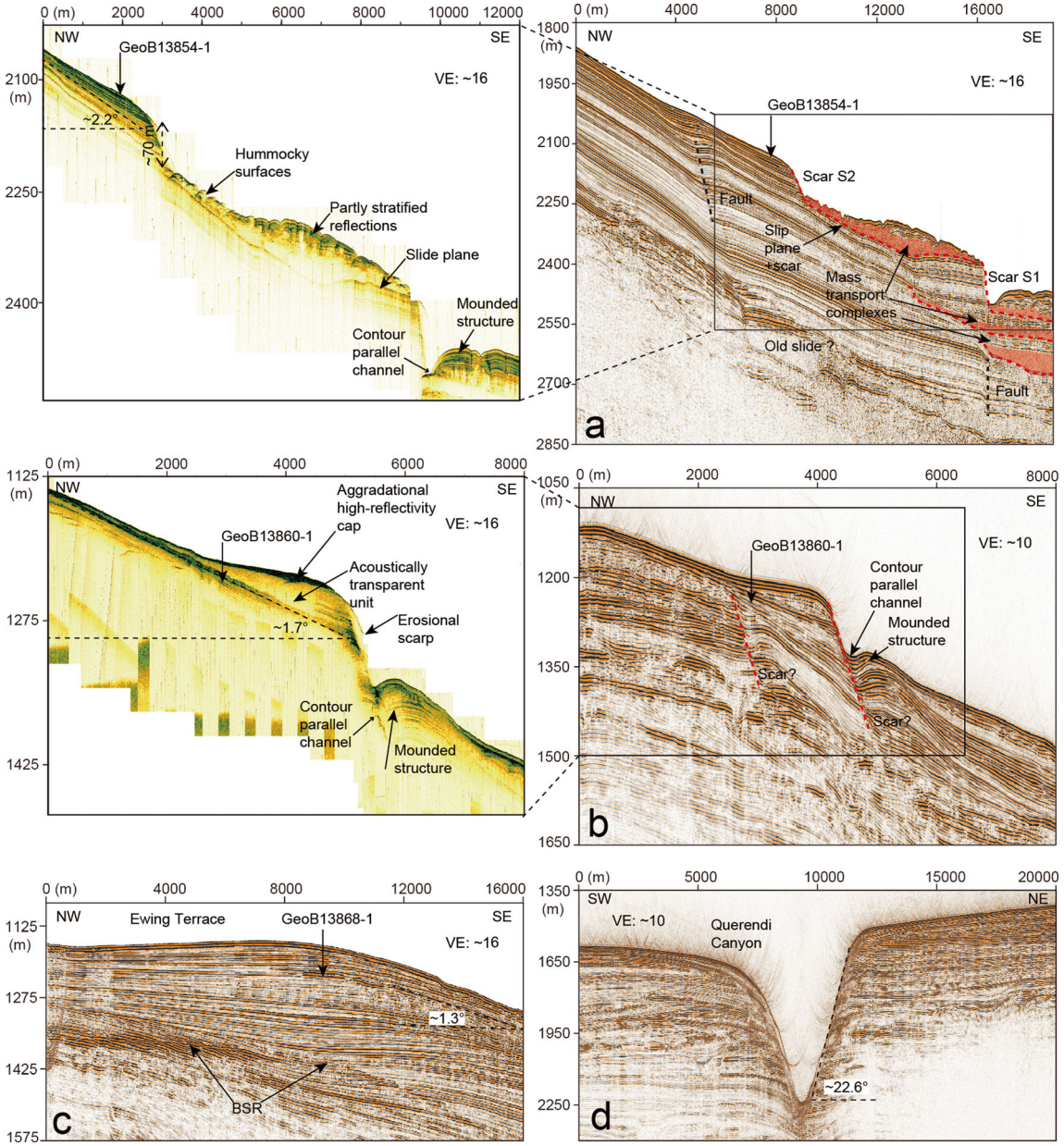

Fig. 2 **a**, **b** Reflection seismic and Parasound profiles of the NS and DS areas respectively. **c**, **d** Seismic profiles of the SC area. For details on seismic acquisition and processing, see Krastel et al. (2011) and Preu et al. (2012); Parasound profile in **b** modified after Krastel et al. (2011)

The southern study area SC is characterized by the nearly flat Ewing Terrace (Fig. 2c), which progressively steepens seawards into a relatively steep slope with inclinations between 3° and 7° (Preu et al. 2013). It formed as a contouritic terrace at the interface between the Antarctic Intermediate Water and Upper Circumpolar Deep Water (Ewing and Lonardi 1971; Preu et al. 2013), and is dissected by canyons without connection to the shelf break (e.g. the Mar del Plata Canyon and Querendi Canyon, Fig. 1). The SC study area focuses on the head region of the Querendi Canyon at ~1,400 m water depth (Fig. 1d). Incision depth in the head region is ~150 m and increases downwards up to 700 m. The headwall is characterized by an amphitheatre-type shape with slope inclinations reaching 37° in places. The lateral canyon slope has inclinations of up to 24° and 21° on the SW and NE flanks respectively, giving rise to a slightly asymmetric canyon profile (Fig. 2d). The width of the canyon is ~2.5 and 8–10 km in the headwall region and further downstream respectively. Most of the canyon area is characterized by a hummocky surface, and MTDs several tens of metres thick have been reported from the thalweg of the Querendi Canyon, hypothesized to indicate retrogressive headward erosion by repeated headwall failures (Krastel et al. 2011).

Today, sedimentation in the greater study area is strongly influenced by high fluvial discharge from the Rio de la Plata and by powerful bottom currents. Sediments generally

comprise hemipelagic clayey silts in the NS and DS study areas and contouritic sandy silts in the SC study area (Huppertz 2011). Recent sedimentation rates may vary depending on position relative to the Rio de la Plata and the contouritic depositional systems, ranging from 80 cm/1,000 years on the open slope in the northern NS area (Henkel et al. 2011) to 160 cm/1,000 years in the Mar del Plata Canyon (Voigt et al. 2013). The study areas are located north and south of the present-day position of the Brazil-Malvinas confluence zone (~37°S), and are in different water depths and thus affected by different water masses. North of the BMC, high quantities of terrigenous sediments (~80×10^6 ton/year) discharged by the de la Plata River, consisting of 75% coarse to medium silt, 15% fine to very fine silt and 10% clay (Giberto et al. 2004), are swept northwards by alongshore currents to be deposited on the Uruguayan continental shelf and slope (Piola et al. 2005); here, sediment transport across the slope is dominated by the southward-flowing North Atlantic Deep Water in water depths of 2,000–4,000 m. South of the BMC, coarse fluvial sediments are trapped within the estuary and occasionally carried directly downslope by turbidity currents (Garming et al. 2005); most of the surficial sediments on the northern Argentinean slope have been reworked and carried northwards by water masses in different depths, including the Antarctic Intermediate Water (~500–1,000 m), the Circumpolar Deep Water (~1,000–3,500 m) and the Antarctic Bottom Water (>3,500 m; for more details, see Piola and Matano 2001).

Materials and methods

The database consists of the results of analyses carried out on sediment gravity cores and MeBo (German for seafloor drilling rig) cores collected during R/V *Meteor* Cruise M78/3 in 2009 (Krastel et al. 2012). The present study focuses on gravity core GeoB13854-1 (core depth of 5.52 m at ~2,120 m water depth) and MeBo core GeoB13860-1 (drill depth of 35.6 m at ~1,220 m water depth with 82% recovery) collected in undisturbed upperslope sediments adjacent to the scars of NS and DS respectively, and MeBo core GeoB13868-1 (drill depth of 21.5 m at ~1,140 m water depth with 34% recovery) from upperslope sediments of SC (Figs. 1 and 2).

Shipboard tests

Visual core description was carried out shortly after core recovery on the split cores. Discrete samples at 50 cm intervals were taken on the working halves to measure the water (moisture) content, bulk density and void ratio using the oven-drying method and a pycnometer (moisture and density, MAD; Blum 1997).

Undrained shear strength (S_u) was estimated by means of a Wykeham Farrance cone penetrometer generally at 10 cm intervals (Wood 1985). Given that the empirical calibration of fall cone penetrometer measurements is based on fine-grained sediments, measurement points were shifted by a few centimetres to avoid sandy sediments in some cases. S_u was also directly measured at 50 cm intervals in fine-grained sediments of cores GeoB13854-1 and GeoB13860-1 using a Mennerich Geotechnik (Germany) vane shear apparatus (rotation 90°/minute; Boyce 1977; Blum 1997), also yielding remoulded undrained shear strength (S_{ur}) and strength sensitivity (S_u/S_{ur}). The two independently measured undrained shear strength datasets enabled order-of-magnitude comparisons and the identification of characteristic strength vs. depth trends.

Laboratory tests

A GeoTeK multi sensor core logger (MSCL) was employed to measure bulk density (by gamma-ray attenuation) and magnetic susceptibility at 2 cm intervals on the archive core halves about 6 months after the cruise. Grain-size analyses were performed using a Beckmann Coulter counter LS 13320 particle size analyzer, which covers a size range from 0.04 μm to 2 mm. Sand, silt and clay contents are represented by the classification scheme of Craig (2004). Atterberg limits including the liquid limit (w_L), plastic limit (w_P) and plasticity index ($I_P = w_L - w_P$) served to distinguish between different types of silts and clays. The liquid limit was determined with a Casagrande apparatus and the plastic limit by the rolling thread method (Casagrande 1932).

To evaluate the consolidation history of the sediments, uniaxial incremental loading oedometer tests were conducted on whole round samples taken at different sub-bottom depths. For this purpose, specimens of 1.5 cm height and 5 cm diameter were trimmed and incrementally subjected to normal loads from 4.9 to 1,962 kPa (ASTM 2004a). Consolidated drained direct shear strength tests were performed using a displacement-controlled direct shear apparatus of Giesa GmbH (Germany) in order to obtain the drained shear strength of the sediments. Specimens of 2 cm height and 5 cm diameter were consolidated at a specified normal load for at least 24 h. After complete dissipation of the excess pore pressure, the specimens were sheared at a shear rate of 0.002 mm/minute for clay and 0.008 mm/minute for silt and sand (ASTM 2004b).

Sample disturbance assessment

Although samples used for the geotechnical analyses were handled with great care, disturbances due to coring effects, transport of sediment cores, and effects of storage time and trimming in the laboratory can nevertheless occur. In order to quantitatively evaluate the degree of disturbance to samples used for consolidation tests (and collocated drained direct shear tests), data from oedometer tests were examined according to two disturbance/quality assessment methods. Silva (1974) defined the disturbance

in percentage of the ratio between Δe and Δe_0, with Δe being the change in void ratio (e) from the initial void ratio (e_0) to the void ratio corresponding to the laboratory compression line, and Δe_0 the change in void ratio from the laboratory compression line to the void ratio at the idealized remoulded baseline. The higher this $\Delta e/\Delta e_0$ ratio, the higher is the degree of disturbance (see Table 1 for definition of disturbance classes). In a related method for assessing sample quality, Lunne et al. (1997) proposed that $\Delta e/e_0$ was more systematically influenced by sample disturbance, with smaller values indicating better sample quality (see Table 1 for definition of quality classes).

Overpressure estimation

Overpressure (Δu), which impacts the effective stress (Terzaghi et al. 1996), is defined as fluid pressure (u) in excess of hydrostatic equilibrium (u_0). Terzaghi's effective stress relationship follows:

$$\begin{aligned}\sigma_{\mathrm{v}}^{'} &= \sigma_{\mathrm{v}} - u = \sigma_{\mathrm{v}} - (u_0 + \Delta u) = (\rho_{\mathrm{b}} - \rho_{\mathrm{w}})gz - \Delta u \\ &= (\gamma - \gamma_{\mathrm{w}})z - \Delta u = \gamma' z - \Delta u\end{aligned} \quad (1)$$

where σ'_{v} is the vertical effective stress, σ_{v} the total overburden stress, ρ_{b} the bulk density, ρ_{w} the water density, γ the unit weight of the bulk sample, γ_{w} the unit weight of water, γ' the buoyant weight, z the overburden depth, and g the acceleration due to gravity. Since the in situ pore pressure of deep-sea sediments is difficult to measure, two methods were used to estimate overpressure in this study. Preconsolidation stress (σ'_{pc}) interpreted from oedometer tests served to estimate overpressure based on Casagrande (1936):

$$\Delta u = \sigma_{\mathrm{vh}}^{'} - \sigma_{\mathrm{pc}}^{'} \quad (2)$$

where σ'_{vh} is the vertical effective stress for hydrostatic conditions ($\sigma'_{\mathrm{vh}} = \gamma' z$). Overpressure due to sedimentation can be evaluated with the Gibson (1958) one-dimensional solution under the assumption of a constant sedimentation rate and an absence of flow along underlying strata. The modelled overpressure is controlled by Gibson's time factor (T_{G}; Flemings et al. 2008):

$$T_{\mathrm{G}} = \frac{m^2 t}{c_{\mathrm{v}}} \quad (3)$$

where m is the sedimentation rate, t represents time, and c_{v} is the coefficient of consolidation defined as $c_{\mathrm{v}} = k / (m_{\mathrm{v}}\gamma_{\mathrm{w}})$. The latter depends on the coefficient of permeability (k) and the coefficient of volume compressibility (m_{v}), both being obtained from oedometer tests.

Slope stability assessment

According to the low average slope angles of the open submarine slopes (1.5–2.5° and <7° in the NS/DS and SC study areas respectively), as well as the low ratio between failure depth (~100 and 150 m in NS/DS and SC respectively) and the spatial extent of slope instability features (20–40 km alongstrike extent of scarps in NS/DS, and 2.5 km width of the canyon in the headwall region in SC), edge effects can be safely ignored and the infinite slope assumption can be employed to calculate the factor of safety (FS) of the slopes (e.g. Biscontin and Pestana 2006). The factor of safety determines whether a given slope is stable (FS>1) or unstable (FS≤1). Slope failure occurs when the failure-inducing stresses acting on the slope exceed the failure-resisting strength of the sediment (Hampton et al. 1996). The shear strength of sediments depends on the conditions and time of drainage during shear. It is essential to consider long-term factors such

Table 1 Sample disturbance/quality assessment using oedometer data following the approaches of Silva (1974) and Lunne et al. (1997): e_0 initial void ratio, Δe_0 laboratory compression line → idealized remoulded baseline, Δe initial void ratio → laboratory compression line. Silva (1974): $\Delta e/\Delta e_0$ <15 very little, 15–30 small, 30–50 moderate, 50–70 much and >70 extreme disturbance. Modified after Lunne et al. (1997): $\Delta e/e_0$ <0.04 very good to excellent, 0.04–0.06 good, 0.06–0.09 fair, 0.09–0.14 poor and >0.14 very poor quality

Area	Core	Depth (m)	e_0	Δe	Δe_0	$\Delta e/e_0$	$\Delta e/\Delta e_0$ (%)	Quality (Lunne et al. 1997)	Disturbance (Silva 1974)
NS	GeoB 13854-1	2.74	1.96	0.13	0.63	0.07	20.6	Fair	Small
		4.71	1.96	0.17	0.54	0.09	32.2	Fair	Moderate
DS	GeoB 13860-1	8.40	1.20	0.06	0.28	0.05	22.4	Good	Small
		12.11	1.06	0.04	0.28	0.04	16.1	Good	Small
		19.33	1.48	0.15	0.37	0.10	39.8	Poor	Moderate
		26.50	1.10	0.05	0.25	0.04	19.3	Good	Small
		33.70	1.24	0.08	0.28	0.06	27.4	Fair	Moderate
SC	GeoB 13868-1	6.23	0.68	0.04	0.10	0.06	39.5	Fair	Moderate
		14.45	0.70	0.03	0.06	0.05	57.6	Good	Much

as overpressure induced by sedimentation (drained condition) and short-term factors (undrained condition) such as forces induced by earthquakes. Slope stability was evaluated for four different scenarios.

Static undrained conditions can be affected by strong change in slope geometry or fluctuation of pore pressure. The factor of safety calculation after Morgenstern (1967) and Løseth (1999) follows:

$$\mathrm{FS} = \frac{S_u}{\gamma' z \sin\theta \cos\theta} \tag{4}$$

where θ is the slope angle (i.e. the assumed angle of the slip surface inferred from reflection seismic profiles in Fig. 2).

Static drained conditions respond to long-term steady-state pore pressure (Dugan and Flemings 2002):

$$\mathrm{FS} = \frac{c' + \gamma' z(\cos^2\theta - \lambda*)\tan\varphi'}{\gamma' z \sin\theta \cos\theta} \tag{5}$$

where c' is the cohesion, φ' the angle of internal friction (both gained from drained direct shear tests) and λ* the overpressure ratio ($\lambda* = \Delta u / \sigma'_{vh}$).

Earthquake undrained conditions use pseudostatic analysis for a simplified evaluation of the seismic factor in slope safety. The earthquake force is represented by a horizontal force and a pseudostatic seismic coefficient (k_e). The pseudostatic acceleration (a) is k_e times the gravitational acceleration g ($a = k_e g$), which is assumed to be applied over a time period long enough for the induced shear stress to be considered constant (Hampton et al. 1996). The undrained pseudostatic factor of safety is given by the following expression (ten Brink et al. 2009):

$$\mathrm{FS} = \frac{S_u}{\gamma' z[\sin\theta\cos\theta + k_e(\gamma/\gamma')\cos^2\theta]} \tag{6}$$

Earthquake drained conditions only include pre-earthquake pore pressure (not considering the overpressure developed during seismic shaking) under the assumption that shear strength does not decrease during seismic shaking:

$$\mathrm{FS} = \frac{c' + \gamma' z(\cos^2\theta - \lambda*)\tan\varphi'}{\gamma' z[\sin\theta\cos\theta + k_e(\gamma/\gamma')\cos^2\theta]} \tag{7}$$

Estimation of peak ground acceleration (PGA)

The critical pseudostatic acceleration (a_c) is the earthquake acceleration at which earthquake-induced stress just equals the shear strength (FS=1 from Eqs. 6 and 7). Critical pseudostatic acceleration, as the average equivalent uniform shear stress imposed by seismic shaking, represents ~65% of the effective seismic peak ground acceleration (PGA = a_c / 65%; Seed and Idriss 1971; Seed 1979; Strasser et al. 2011). The median ground motion of peak ground acceleration was estimated using the empirical seismic attenuation relationship of Campbell and Bozorgnia (2008). Absolute PGA values depend on earthquake magnitude, source distance, style of faulting, etc. Here, only the former two well-known parameters served for PGA determination:

$$\ln\mathrm{PGA} = \begin{cases} (c_0 + c_1 M) + \left[(c_4 + c_5 M)\ln\left(\sqrt{R_{\mathrm{RUP}}^2 + c_6}\right)\right], & M \le 5.5 \\ (c_0 + c_1 M) + c_2(M - 5.5) + \left[(c_4 + c_5 M)\ln\left(\sqrt{R_{\mathrm{RUP}}^2 + c_6}\right)\right], & 5.5 < M \le 6.5 \\ (c_0 + c_1 M) + c_2(M - 5.5) + c_3(M - 6.5) + \left[(c_4 + c_5 M)\ln\left(\sqrt{R_{\mathrm{RUP}}^2 + c_6}\right)\right], & M > 6.5 \end{cases} \tag{8}$$

where M is the earthquake magnitude, R_{RUP} is the epicentral distance, and $c_{0–6}$ are empirical coefficients equal to –1.715, 0.5, –0.53, –0.262, –2.118, 0.17 and 5.6 respectively (Campbell and Bozorgnia 2008).

Results

Physical and geotechnical sediment properties

Visual core description shows that the sediments at the NS and DS sites (cores GeoB13854-1 and GeoB13860-1) consist mainly of fine-grained material (silt and clay) with interbedded sand layers, whereas those of the SC site (core GeoB13868-1) are characterized by contouritic facies associations including very fine to medium sand (Fig. 3). Magnetic susceptibility provides a first-order estimate of ferromagnetic mineral abundance in sediments and is sensitive to grain-size variations (e.g. Bozzano et al. 2011), with higher grain size resulting in higher magnetic susceptibility in the cores of the present study (Fig. 3).

Grain-size distributions and Atterberg limits from whole round samples give a more refined classification for sediments (Fig. 4). The representative grain size of sediments from NS and DS is clayey silt (~20% clay, 10–20% sand) to sandy silt

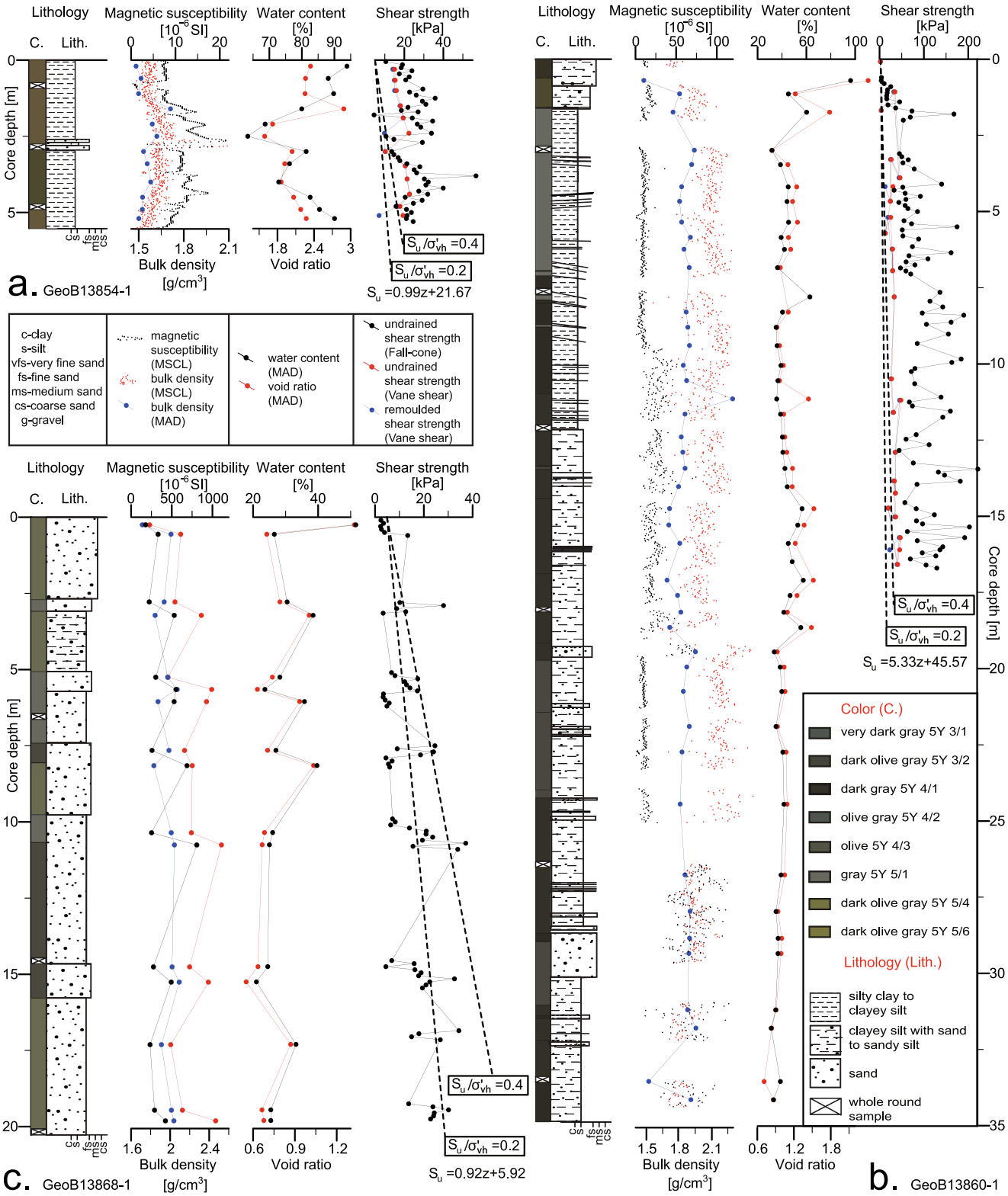

Fig. 3 Physical and geotechnical properties of sediments from the NS (**a** core GeoB13854-1), the DS (**b** core GeoB13860-1) and the SC areas (**c** core GeoB13868-1). Dashed lines in undrained shear strength plots: S_u/σ'_{vh} ratios showing trends of underconsolidation, normal consolidation and overconsolidation (≤0.2, 0.2–0.4 and ≥0.4 respectively). GeoTeK MSCL-based magnetic susceptibility and bulk density of GeoB13868-1: mean value per core section, because of drilling-induced disturbance of sandy material containing heavy minerals

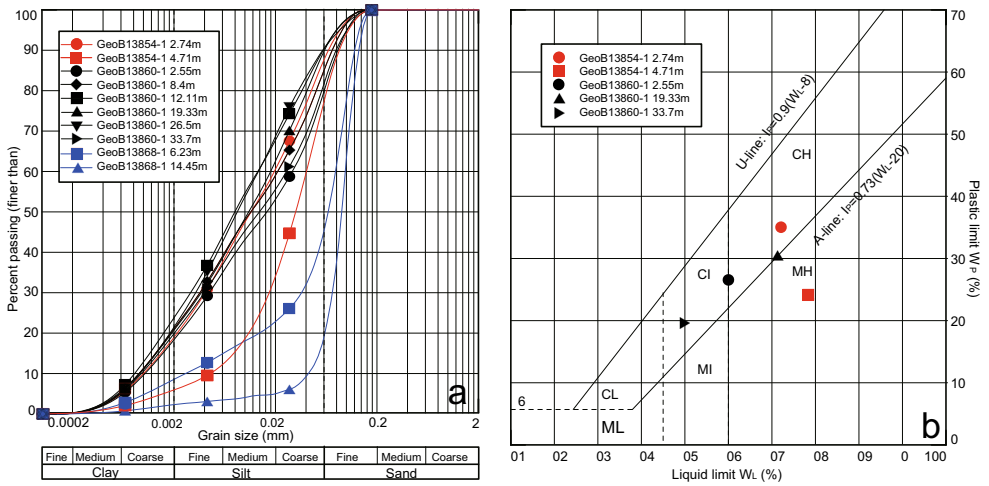

Fig. 4 **a** Grain-size distributions of sediments from the NS (core GeoB13854-1), DS (GeoB13860-1) and SC areas (core GeoB13868-1). **b** Plasticity chart for fine-grained sediments of the NS and DS areas (classification modified after Craig 2004). The *A-line* separates clays (C) from silts (M); *U-line* approximate upper limit of w_L and w_P combinations for natural soils. *CH, CI and CL* Inorganic clays of high, intermediate and low plasticity respectively; *MH, MI and ML* inorganic silts of intermediate–high, intermediate and low plasticity respectively

(core GeoB13854-1 at 4.71 m) with intermediate to high plasticity. The representative grain size of sediments from SC is silty sand (2–8% clay, 18–38% silt).

The bulk density values obtained from MAD are generally slightly lower than those obtained from MSCL (Fig. 3). Silty sediments from NS and DS show lower bulk densities (1.5–2.1 g/cm^3) compared to sandy sediments from SC (1.7–2.4 g/cm^3). The high water contents (65–95%) near the surface (GeoB13854-1 at 5 m) decrease strongly to ~20% at greater depth (GeoB13860-1 at 35 m). The sandy sediments (GeoB13868-1) from SC, by contrast, have overall lower water contents ranging from 20–50%. Void ratios show similar trends with highest values (1.6–3.0) in core GeoB13854-1 and lowest ones (0.6–1.2) in core GeoB13868-1.

Undrained shear strengths from vane shear tests are slightly lower than the values from cone penetrometer measurements at a given depth (Fig. 3). Sediments of core GeoB13854-1 have high undrained strength (~20 kPa) near the top of the core, and the values gradually increase to ~30 kPa at 5 m core depth. The coarse-grained sediments in the top 1.5 m of core GeoB13860-1 have low shear strengths (0–20 kPa), but these increase strongly as the sediment gets finer, reaching values of up to ~200 kPa down to 16 mbsf (metre below seafloor). Undrained shear tests were not carried out below 16 mbsf because the sediments were too stiff or even hard. The strength sensitivity of the sediments from NS and DS obtained from vane shear tests is low (1.0–2.7). Vane shear tests were not conducted on the sandy sediments from SC because undrained tests cannot be performed in such sandy sediments. The shear strength measurements obtained by cone penetrometer on core GeoB13868-1 range from ca. 0 to 30 kPa. The ratio of the undrained shear strength to vertical effective stress (S_u/σ'_v) gives an indication of the consolidation state of the sediment. Typical values for normally consolidated sediments range from 0.2–0.4 (Locat and Lee 2002). Sediment stiffness at a given depth indicates that the material at the NS and DS sites is highly overconsolidated, whereas that at the SC site is underconsolidated to normally consolidated.

Results of the oedometer test are presented in Table 2, and Fig. 5a shows plots of void ratio versus applied vertical effective stress (the latter along a logarithmic scale). Samples from core GeoB13854-1 (NS site) show a large amount of compression (decrease in void ratio from 2 to 0.6), whereas samples from core GeoB13868-1 (SC site) show comparatively little compression (decrease in void ratio from 1 to 0.6). The preconsolidation stress, which is the maximum effective stress the sediments have ever been subjected to, was determined by the classical graphic method of Casagrande (1936). The overconsolidation ratio, OCR (ratio of preconsolidation stress to present-day overburden effective stress), has been calculated to range between 1.74 and 0.14 for NS and DS sediments (with the exception of a shallow subsurface sample from gravity core GeoB13854-1 suggesting an OCR of 12.73), and between 1.49 and 0.13 for SC sediments. The compression index (C_c), a measure of sediment compressibility, shows an intermediate compressibility (C_c = 0.30–0.39) for the upper 5 m of core GeoB13854-1 and low compressibility (C_c = 0.12–0.26) down to 35 mbsf in core GeoB13860-1 for the dominantly silty material from the NS and DS sites. Very low compressibility (C_c = 0.014–0.039), by contrast, is found for the sandy sediments from the SC site. Coefficients of consolidation (c_v), a measure of the rate at which sediment consolidates, are relatively low (c_v = 1.1e^{-8}–2.2e^{-7} m^2/s) for NS/DS materials and higher (c_v = 6.0e^{-8}–2.9e^{-6} m^2/s) for SC materials. The vertical coefficients of permeability (k), which were back-calculated from c_v, are presented as plots of void ratio versus coefficient of permeability (the latter along a logarithmic scale; Fig. 5b). The values lie in the

Table 2 Summary of laboratory oedometer test results: ρ_b bulk density, σ'_{vh} hydrostatic vertical effective stress, σ'_{pc} preconsolidation stress, OCR overconsolidation ratio, C_c compression index, c_v coefficient of consolidation, k coefficient of permeability

Area	Core	Depth (m)	ρ_b (g/cm^3)	σ'_{vh} (kPa)	σ'_{pc} (kPa)	OCR	C_c	c_v (m^2/s)	k (m/s)
NS	GeoB13854-1	2.74	1.57	15.32	195	12.73	0.389	8.8e^{-08}	8.9e^{-10}
		4.71	1.56	25.92	45	1.74	0.304	1.1e^{-08}	3.6e^{-10}
DS	GeoB13860-1	8.40	1.82	67.32	75	1.11	0.148	5.7e^{-08}	5.2e^{-10}
		12.11	1.86	102.29	20	0.20	0.143	2.2e^{-07}	2.3e^{-09}
		19.33	1.83	157.20	190	1.21	0.256	7.1e^{-08}	5.0e^{-10}
		26.50	1.84	217.85	32	0.15	0.125	5.2e^{-08}	4.7e^{-10}
		33.70	1.84	279.02	40	0.14	0.145	4.9e^{-08}	2.8e^{-10}
SC	GeoB13868-1	6.23	1.88	53.60	80	1.49	0.039	6.0e^{-08}	2.6e^{-10}
		14.45	1.96	135.52	18	0.13	0.014	2.9e^{-06}	3.0e^{-09}

range of 3.6e^{-10}–2.3e^{-9} m/s for NS/DS sediments and 2.6e^{-10}–3.0e^{-9} m/s for SC sediments.

Overpressures estimated from preconsolidation stress have ratios of 0.8–0.86 in NS/DS and ~0.87 in SC, suggesting that non-equilibrium consolidation occurs in all study areas. Using Gibson's analytical solution for consolidation, the degree of overpressure controlled by Gibson's time factor (Eq. 3) is reported in Table 3. Although previous studies have shown high sedimentation rates (0.8–1.8 m/1,000 years) in recent deposits of NS (Henkel et al. 2011) and also high rates (up to 1.6 m/1,000 years) along the thalweg of the canyon of SC during the Holocene (Voigt et al. 2013), a reliable long-term sedimentation rate for the general study area is still lacking. In the present case, a lower sedimentation rate of 0.1 m/1,000 years has been selected, this being more plausible for averaging long-term sedimentation on the open slope (NS/DS) and in the contourite depositional systems (SC; e.g. Krastel et al. 2011; Preu et al. 2012, 2013). Calculations are based on a

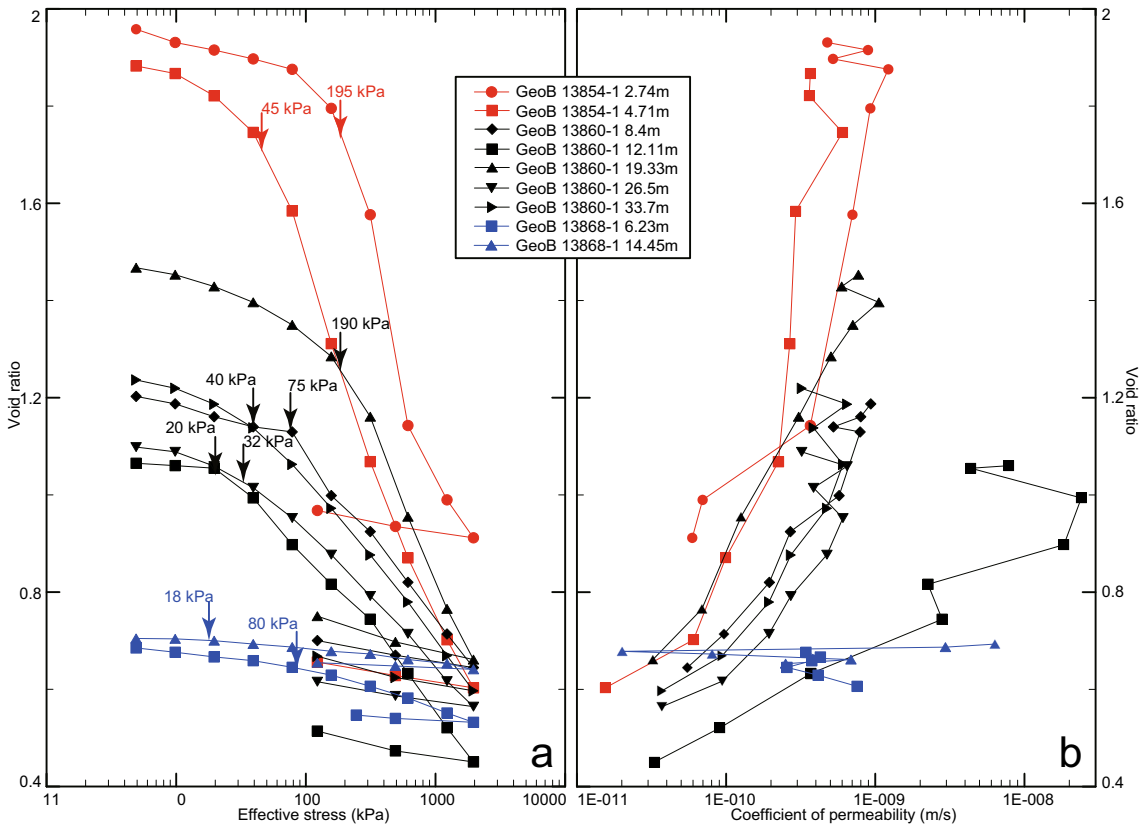

Fig. 5 **a** Void ratio (e) vs. vertical effective stress (σ'_{vh}) relationships from oedometer tests with calculated preconsolidation stress (σ'_{pc}) for the NS/DS (cores GeoB13854-1 and GeoB13860-1) and SC areas (core GeoB13868-1). **b** Corresponding void ratio (e) vs. coefficient of permeability (k) plot. Note the logarithmic scales of both X axes

Table 3 Gibson parameters for overpressure estimation: c_v coefficient of consolidation, m sedimentation rate, t duration of consolidation, T_G Gibson time factor, λ^* overpressure ratio

Area	Core	c_v (m^2/s)	m ($m/10^3$ years)	t (10^3 years)	T_G	λ^*
NS	GeoB13854-1	$1.57e^{-08}$	0.1	500	10.07	0.6
DS	GeoB13860-1	$4.17e^{-08}$	0.1	500	3.80	0.5
SC	GeoB13868-1	$1.30e^{-07}$	0.1	500	1.22	0.3

time span of 500,000 years for all study areas (cf. estimated overpressure at 50 mbsf). Average coefficients of consolidation were obtained by oedometer tests. The results of overpressure ratio estimated by contour plots of Gibson's time factor show overpressure ratios ranging between 0.5–0.6 in NS/DS and of ~0.3 in SC.

Drained direct shear test results (Table 4) are presented as plots of shear stress versus horizontal displacement (Fig. 6, panel a), and shear strength versus effective normal stress to construct the Mohr-Coulomb failure envelope (Fig. 6, panel b). The stress–displacement profiles for the NS/DS sediments are characterized by smooth peaks without subsequent drops in shear stress, whereas the SC sediments are characterized by distinct peaks followed by drops in shear stress. Values of the effective cohesion intercept (c') range from 1.5–20.1 kPa in NS/DS sediments and 12.9 kPa in SC sediments. Lower values (30.3–34.3°) of the angle of internal friction (φ') are found in the fine-grained sediments from NS/DS, as compared to those (36.9–41.3°) in the coarse-grained sediments from SC.

Evaluation of geotechnical data quality and interpretation

The results of the geotechnical laboratory tests presented above are only an approximation of actual in situ conditions, and can be biased by sample disturbance or methodological constraints. For instance, during sampling of granular sediments such as the silty sands in the SC area, pore fluids may squeeze out of the sampled volume, resulting in volume reduction. This could be a possible explanation why density values obtained from the MAD method are slightly lower than those obtained from MSCL. Also, the partly granular nature of the contouritic sediments in the SC area may have resulted in partial drainage of fluid upon fall cone penetration. Although care was taken to perform these tests only in fine-grained sediments, partial drainage may explain the relatively low S_u values from core GeoB13868-1 because the fine-grained contouritic facies can have sand contents up to 10%. Undrained shear strengths derived from vane shear tests are lower than those from cone penetrometer measurements at the same depth. This is interpreted to reflect the different physics on which the two methods are based in deriving the compressional strength (approximated as shear strength in the fall cone tests, after Wood 1985), on the one hand, and the strength from shear deformation in the vane shear test (Blum 1997), on the other.

Table 4 Summary of direct shear test results: c' cohesion, φ' angle of internal friction

Area	Core	Depth (m)	c' (kPa)	φ' (°)
NS	GeoB13854-1	0.74	1.52	34.25
		4.71	7.59	31.72
DS	GeoB13860-1	2.55	6.33	33.34
		19.33	11.53	30.55
		33.70	20.07	30.31
SC	GeoB13868-1	6.23	12.91	36.89
		14.45	12.92	41.30

Results of sample quality assessment are shown in Table 1. The method proposed by Silva (1974) indicates that most analyzed samples have experienced small to moderate disturbance, whereas the method proposed by Lunne et al. (1997) classifies the quality of most samples as "good" or "fair" Only two samples indicate strong disturbance and poor sample quality (GeoB13860-1, 19.33 m; GeoB13868-1, 14.45 m). Neither of these two samples shows outlier values in the oedometer or direct shear experiments, although the relatively high angle of internal friction φ'=41.3° for the samples from the sandy contouritic deposits in GeoB13868-1, 14.45 m might have been compromised by sample disturbance and, thus, has to be interpreted with caution. Since sample quality is not excellent throughout, but rather moderate to good, and since the shape of the void ratio–effective stress (log scale) relationship does not always enable a profile-specific definition of the zone of maximum curvature, absolute values of the presented oedometer data have uncertainties up to 30%, whereas relative trends are considered as reliable. In particular, the very low OCR values suggested by some of the tests could result from having inferred "disturbed" preconsolidation stresses, which do not reflect the in situ conditions correctly. This has direct implications for the overpressure estimates based on preconsolidation stresses, and might explain why those estimates show generally higher overpressure ratios than the estimates from the contour plots of Gibson's time factor.

In contrast to the interpretation that samples with particularly low OCR values are potentially affected by sample disturbance, the very high OCR value of 12.73 from 2.74 m

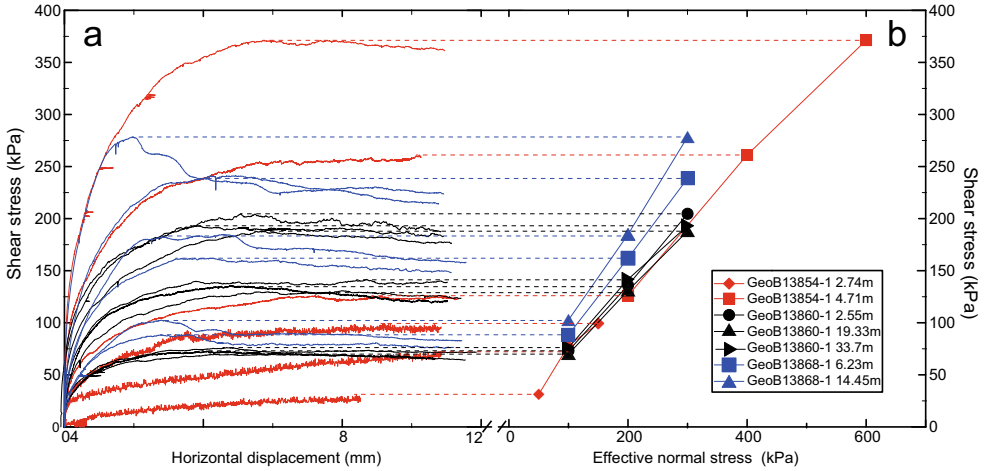

Fig. 6 *Panel a* Direct shear test protocols showing shear stress vs. horizontal displacement for the NS (core GeoB13854-1), DS (core GeoB13860-1) and SC areas (core GeoB13868-1). *Panel b* Mohr-Coulomb failure planes at peak shear strengths

below seafloor at site GeoB13854-1 can be explained by the effect of apparent overconsolidation. This is typical for the uppermost section of most marine deposits which have cohesion strengths exceeding those of preconsolidation stress, the latter being due to weak interparticle bonds or bioturbation (Lee et al. 1999).

Slope stability analysis

For the slope stability calculations, factors of safety for four different scenarios were calculated using Eqs. 4 to 7 with two parameters changing within a certain range and other parameters being kept constant (Table 5, Fig. 7). The values defining the present-day situation serve to constrain the factors of safety for undrained and drained static scenarios, revealing that the slopes are today stable in both cases. Since slope geometry plays an important role in slope instability, variable slope angles (1–5°) and variable failure depth levels (10–100 m) were used to calculate FS for the undrained static case. The undrained shear strength–depth relation was obtained using cone penetrometer data with linear regression. Seeing that these data might be slightly underestimating the actual in situ conditions (particularly for the SC study area; see subsection above), the slope stability scenarios would rather be conservative estimates of potential instabilities (cf. slope stability might be slightly higher under in situ conditions).

The results indicate that slope failure depth has less influence on stability than does slope angle. For other scenarios with an assumed slope failure depth of 50 mbsf, slopes are stable in the undrained static case. SC is vulnerable with FS in the order of 1–2, although low FS values correlated with low undrained shear strength values, which probably underestimate in situ strength conditions (see subsection "Evaluation of geotechnical data quality and interpretation" above). For the

Table 5 Parameters used for slope stability calculations: US undrained static, DS drained static, UE undrained earthquake, DE drained earthquake

Parameters	NS area				DS area				SC area			
	GeoB13854-1				GeoB13860-1				GeoB13868-1			
	US	DS	UE	DE	US	DS	UE	DE	US	DS	UE	DE
S_u (kPa)	0.99z+21.67		71.17		5.33z+45.57		312.07		0.92z+5.92		51.92	
z (m)	10–100	50			10–100	50			10–100	50		
β (°)	1–5				1–5				1–5			
c' (kPa)	-	4.5	-	4.5	-	12.5	-	12.5	-	13.0	-	13.0
φ' (°)	-	32.5	-	32.5	-	30.5	-	30.5	-	40.0	-	40.0
λ*	-	0–0.9	-	0.5	-	0–0.9	-	0.5	-	0–0.9	-	0.5
γ (kN/m^2)	-	-	15.21		-	-	18.05		-	-	19.23	
k_e	-	-	0–0.09	0–0.15	-	-	0–0.36	0–0.15	-	-	0–0.06	0–0.21
γ' (kN/m^2)	5.21				8.05				9.23			
g (m/s^2)	9.81				9.81				9.81			
FS/k_e	7.2/-	8.8/-	1/0.08	1/0.125	26/-	10/-	1/0.34	1/0.13	4.9/-	19.5/-	1/0.043	1/0.20

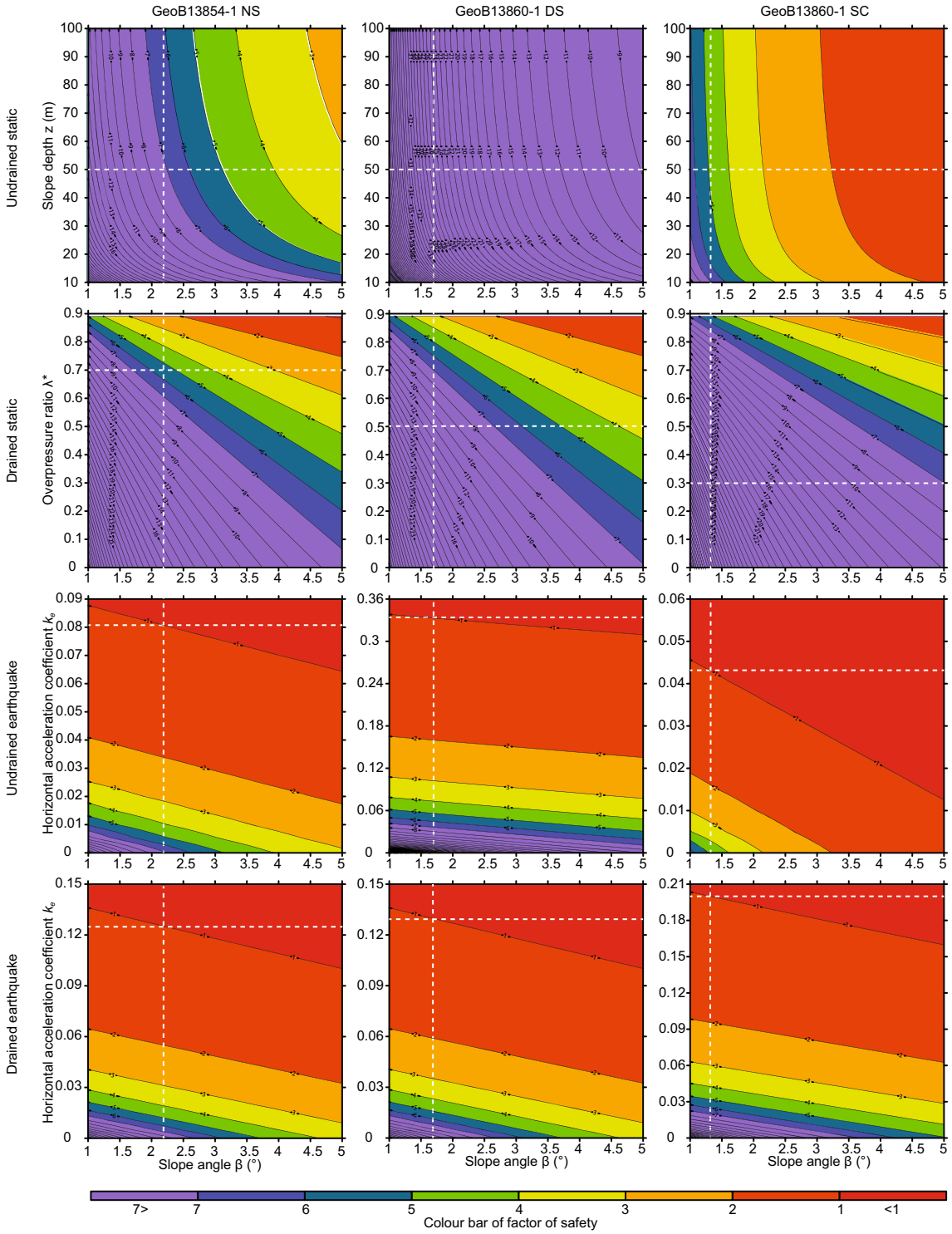

Fig. 7 Slope stability analyses showing variations in the factor of safety (FS) as a function of slope angle under undrained and drained static as well as earthquake scenarios for the NS (core GeoB13854-1), DS (core GeoB13860-1) and SC areas (core GeoB13868-1). *Dashed white lines* Present-day mean values of parameters for static analyses, and pseudostatic horizontal acceleration required to trigger slope failure (FS=1) at present-day mean slope angles for pseudostatic analyses (see Table 5 for input parameters, and main text for further explanations)

drained static case, different overpressure ratios (0–0.9) and different slope angles (1–5°) were chosen for FS calculations. The results indicate that overpressure is unlikely to trigger slope failure in static scenarios. Factors of safety for the NS and DS areas tend to be lower compared to the undrained situation, the reverse being the case for the SC area.

Pseudostatic infinite slope stability analysis represents a first-order estimation of seismic ground accelerations which

affect a given slope. The minimum horizontal acceleration coefficient required to trigger slope failure (FS=1) was back-calculated based on Eqs. 6 and 7. For the undrained earthquake case, high values of horizontal acceleration, i.e. k_e=0.08 and 0.34, are needed to trigger slope failure in the NS and DS areas respectively, whereas a low value (k_e=0.04) is needed to trigger slope failure in the SC area. Given the scatter in the overpressure estimates and the possibility that high overpressure ratios estimated from uniaxial consolidation tests might be biased towards excessively high values by samples with moderate disturbance, a value of 0.5 was assumed in the drained earthquake case for all areas. The results for SC indicate that a higher horizontal acceleration (k_e=0.20) is required in the drained case compared to the undrained case. For NS the horizontal acceleration is slightly higher (k_e=0.13) in the drained scenario, whereas for DS a substantial difference is observed (k_e=0.34 vs. 0.13) between the undrained and drained case.

Discussion

Preconditioning factors

Preconditioning factors are defined as the physical and geotechnical properties of sediments resulting from initial deposition and post-depositional alteration, which promote slopes to be susceptible to instability. Physical and geotechnical sediment properties depend to a large extent on lithology and grain size, the latter determining the pore volume-controlled properties (e.g. bulk density, water content, void ratio; Baraza and Ercilla 1994). For undrained analysis, shear strength mainly depends on the grain size and stress history of the sediment. Thus, already small increases in sand content can notably decrease the undrained shear strength (Lee et al. 1987). A high overconsolidation ratio commonly results in higher undrained strength (Hampton et al. 1996). When translating these findings to the present study, undrained slope stability analyses attest that the southern-canyon (SC) area is vulnerable because of its lower undrained shear strength caused by the coarse-grained nature of the sediments, whereas the open Uruguayan slope (NS and DS areas) is more stable because of the higher undrained shear strength caused by the fine-grained nature of the sediments (see Fig. 3). Even when considering uncertainties in absolute physical terms due to sampling and measurement effects (see subsection "Evaluation of geotechnical data quality and interpretation" above), this finding should be robust and highlights that the primary sedimentological differences between the two study sectors is also expressed by different slope stability conditions and modes of slope failures.

For drained analysis, the shear strength is governed by cohesion (c'), angle of internal friction (φ') and effective vertical stress (σ'_v). Cohesion is regarded as a physicochemical component of shear strength which is independent of the effective stress (Lamb and Whitman 1969). In general, fine-grained materials have higher cohesion compared to coarse-grained materials. On the other hand, the presence of fine-grained materials can be an important control parameter for lower angles of internal friction (Huhn et al. 2006). In the present study, the lowest φ' was measured for clayey sediments, whereas sandy sediments showed stronger frictional strength from the direct shear test. This trend holds even if the high φ' value of 41.3° for core GeoB13868-1 (14.45 m) is rejected because of poor sample quality (see subsection "Evaluation of geotechnical data quality and interpretation" above). This supports the present findings that the contouritic deposits in the SC area are more stable under drained conditions than the finer-grained slope sediments in the NS and DS areas.

Effective vertical stress σ'_v is determined by sediment pore pressure. Some factors (e.g. high sedimentation rates, the presence of gas bubbles, gas hydrate dissociation and fluid seepage) could result in overpressure (e.g. Sultan et al. 2004). In the present case, pore pressure predictions from the oedometer are probably biased towards too high values (see subsection "Evaluation of geotechnical data quality and interpretation" above) and those estimated from Gibson's time factor rely on uncertainties of long-term sedimentation rates, for which no reliable data are available in the study areas. However, conceptually, overpressure induced by sedimentary processes largely depends on permeability, which also depends on sediment grain size. The slope sediments of NS and DS have a lower permeability than do the contouritic sediments of SC, mainly because of grain-size differences. Therefore, overpressure development is expected to be more critical on the Uruguayan open slope than in the SC area. This interpretation is supported by a comparison between the average slope angles of failure scars (10–20° for the NS and up to 37° for the SC) and the internal angles of friction (~31 and 37° for the NS and SC respectively): the low slope angles (i.e. lower than the friction angle) within the scar headwall in the NS area could indeed indicate the presence of excess pore pressure according to the Mohr-Coulomb failure criteria. The slope stability analyses, however, suggest that the slopes appear to be stable under both undrained and drained static situations today, even if assuming long-term overpressure development in the NS area. Hence, additional triggers would be needed to cause slope failure.

Triggering mechanisms

Triggering mechanisms are termed external stimuli which initiate slope instability processes (Sultan et al. 2004). Compared to preconditioning factors, these occur on shorter timescales. For instance, earthquakes are known to trigger

large submarine mass movements by imposing horizontal acceleration which is usually confined to undrained conditions (Locat and Lee 2002). When considering earthquake-induced acceleration as a static parameter, it is reasonable to also evaluate scenarios for a drained pseudostatic model (Mulder et al. 1994). Of the present study sites, SC is more vulnerable in an undrained scenario where a 0.066 *g* value of effective earthquake peak ground acceleration (PGA = 0.043 *g* / 0.65) is sufficient to trigger the slope failure. As discussed in the subsection "Evaluation of geotechnical data quality and interpretation" above, however, these very low values need to be considered with caution. For the NS area, PGA in the order of 0.12–0.19 (k_e=0.08–0.125) is required to trigger the slope failure under undrained as well as drained conditions.

In order to further explore plausible scenarios for such earthquake events which might induce seismic shaking in this intensity range along the Argentinean–Uruguayan margin, PGA is estimated using an empirical attenuation equation after Campbell and Bozorgnia (2008), which depends on the combination of magnitude and source distance of a given earthquake. In general, the study area shows low seismic activity (Fig. 1a) and, over the past 160 years, only one earthquake of magnitude 5.2 has been reported (in 1988). The epicentre was located 20 km from the GeoB13860-1 and 80 km from the GeoB13854-1 core sites. The PGA induced by this earthquake (0.06 *g*) is too low to even trigger instability at site GeoB13860-1, which is nearest to the presumed epicentre (Fig. 8). The attenuation relationship indicates that moderate *M*4 near-field events in epicentre distances <6 km or very rare strong earthquakes (e.g. *M*7) in the far-field are required to trigger slope failure on the open Uruguayan slope. This assessment thus discounts the 1988 earthquake as a potential slope failure mechanism.

An alternative trigger mechanism may be slope oversteepening: Since slope stability typically decreases with increasing slope angle, slope failures can also be triggered either by rapid asymmetric sediment accumulation on the upper slope or by erosion of the slope toe by bottom currents. The SC study area shows evidence for contour current-induced processes, featuring both high sedimentation rates (up to 1.6 m/1,000 years) during the Holocene (Voigt et al. 2013) as well as high current speeds continuously reworking the base of the canyon flanks. Similarly, the scour below the scarp in the DS area (Fig. 1c) points to strong currents eroding the base of the scarp which may have repeatedly triggered small-scale landslides, the deposits of which may subsequently have again been remobilized by the strong currents. This interpretation would explain why no larger MTD is found below the SD scarp (Fig. 2b). The presence of strong contour currents therefore suggests that slope oversteepening by current-induced erosion may be an important mechanism triggering small-scale landslides in this setting.

Slope failure modes: open slope vs. canyon

In general, low-gradient margins tend to have high sediment inputs and only few canyons, whereas high-gradient margins tend to have lower sediment inputs but more canyons (O'Grady et al. 2000). Low-gradient settings often promote large-scale, though infrequent, slope failures because of thick

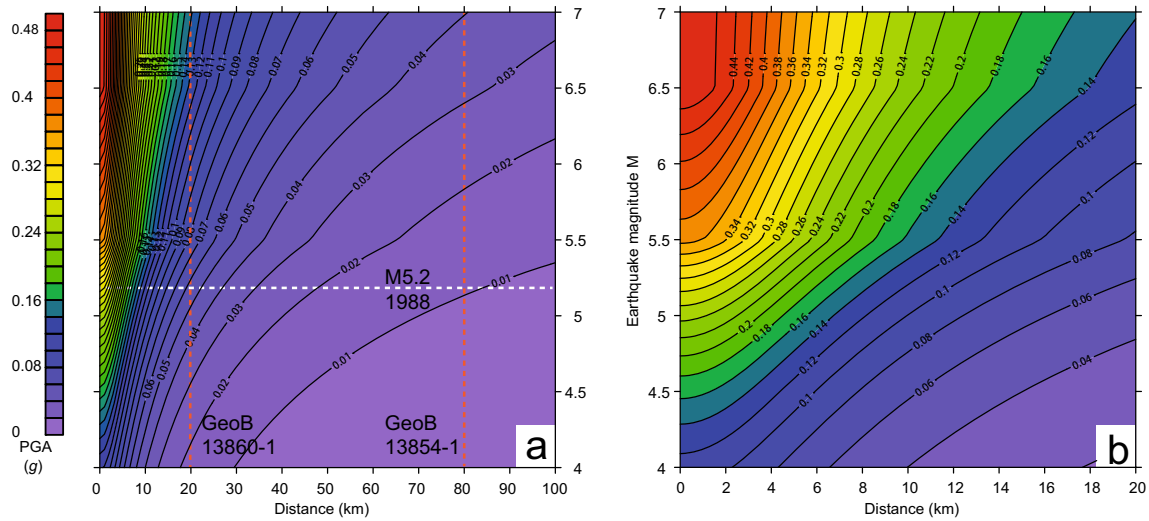

Fig. 8 **a** Estimated peak ground acceleration (PGA, as fraction of gravitational acceleration *g*; cf. empirical attenuation equations of Campbell and Bozorgnia 2008) as a function of earthquake magnitude (*M*4–*M*7) and source distance (0–100 km). *Dashed white line* Presumed magnitude (*M*5.2) of 1988 earthquake. *Dashed red lines* Distances between the two slope sectors examined in the NS and DS areas and the presumed location of the 1988 earthquake epicentre, i.e. ca. 80 and 20 km for cores GeoB13854-1 and GeoB13860-1 respectively. **b** Zoom-in at 0–20 km source distance for PGA reported in **a**

unstable sediment accumulations which build up over long time periods. High-gradient settings, by contrast, promote more frequent small-scale failure events which prevent thick unstable sediment accumulations to build up (Migeon et al. 2011). Since canyons are important conduits for focused sediment transport by turbidity currents, the absence of major canyon systems on open slopes promotes widespread sediment accumulation (Locat and Lee 2009).

The Uruguayan continental slope is characterized by low slope gradients (1–3°) and large expanses of fine-grained sediments. Northward-flowing bottom currents transporting fine-grained sediments from the Rio de la Plata progressively decrease in velocity, thereby promoting the formation of clayey contourites on the slope. As a consequence, large-scale submarine landslide complexes with high headwalls (up to 100 m) and MTDs deposited at the foot of scarps occur repeatedly. The seismic structures of the NS slope failure complex (Fig. 2a) reveal deeply buried MTDs associated with scar S1 on the lower slope, scar S2 with younger MTDs upslope of S1, and seaward-dipping discontinuities even further upslope, possible indicating incipient fronts of future slope failures. This geometry is interpreted to represent a retrogressive slope failure system in which successive landslides are dislocated progressively farther upslope (Krastel et al. 2014). The slope stability analyses of this article suggest that the NS area is today stable and unlikely to experience repeated small-scale failures in the foreseeable future. This does not exclude the possibility that it may nevertheless reach a large-scale unstable state if external triggers (e.g. earthquakes) are strong enough. This interpretation is consistent with a general model of a low-gradient continental slope characterized by high sedimentation of fine-grained sediments and infrequent large-scale slope failures.

The continental slope between 1,400–2,500 m in the SC area, by contrast, is characterized by steep slopes (3–7°) and more abundant coarse-grained sediment on the flat Ewing Terrace, which on the upper slope is dissected by the Querendi Canyon. In this case, the slope stability analyses outlined above attest to a generally low stability characterized by repeated small-scale slope failures triggered by slope oversteepening and by infrequent seismic events. Strong bottom currents are responsible for the accumulation of asymmetrical sandy contourites on the upper slope of the steep Querendi Canyon, where they become unstable and are redeposited within the canyon. Thus, whereas MTDs are found in the mouth of the canyon, they are absent in the upper part of the canyon (Krastel et al. 2011). This suggests that the material continuously eroded in the course of small slope failures along the steep headwall is efficiently evacuated along the channel. As a consequence, the flanks of the canyon are constantly being reshaped by wall incisions which laterally retrograde into the adjacent open slope.

Comparison with slope failures on other passive margins

An important result of this study is the finding that the investigated slopes along the Uruguayan and northern Argentinean margin are mostly stable under static loading conditions and that slope failures require additional driving forces such as earthquakes. This suggests that rare earthquakes may play a critical role in initiating slope failure even along passive margins characterized by generally low seismicity. Similar conclusions have been reached from seismic slope stability analyses in intraplate settings worldwide, such as the upper slope of north-eastern Australia (Puga-Bernabéu et al. 2013), the Gela Basin in the central Mediterranean Sea (Ai et al. 2014), the northern Gulf of Mexico (Stigall and Dugan 2010) and the Norwegian continental slope (Storegga slide; Leynaud et al. 2004, 2009). Due to different precondition factors in different geographic settings (e.g. slope gradient, overpressure, grain size, presence of an intrinsically weak layer), critical peak ground accelerations generated by earthquakes needed to initiate slope failure range between 0.02 *g* for the Gulf of Mexico (Stigall and Dugan 2010), 0.03–0.08 *g* for the Gela Basin (Ai et al. 2014) and 0.1–0.2 *g* in the vicinity of the Storegga slide (Kvalstad et al. 2005).

These case studies further attest to the fact that overpressure generated by strong sedimentation rates is important to precondition the slope towards lower stability (e.g. Sultan et al. 2004) but, in most cases, overpressure alone does not cause slope failure (Kvalstad et al. 2005; Stigall and Dugan 2010). Assuming overpressure ratios are 0.5–0.6 (estimated using Gibson's equation by integrating sedimentation rate and permeability) in the upper 50 mbsf in the NS area of the present study, PGAs exceeding 0.19–0.2 *g* are required to trigger sediment failure. This suggests "triggering conditions" similar to those for the Storegga landslide, where weak layers have been identified in contouritic deposits which formed during interglacial periods and were subsequently rapidly buried under thick glacial marine deposits (Bryn et al. 2005). These fine-grained contouritic deposits are probably responsible for the staircase appearance of headwalls and the retrogressive nature of the Storegga slope failure. Offshore Uruguay and northern Argentina, bottom currents are inferred to be responsible for the distinct morphologies of the NS, DS and SC areas (Preu et al. 2013). The strong currents control the sedimentation pattern which, in turn, exerts a key control on the slope stability precondition. The influence of contour currents on mass wasting processes and the shaping of continental margins has also been highlighted by a recent comparison between submarine landslides off NE Africa and Uruguay/Argentina (Krastel et al. 2014), showing that contouritic depositional systems feature smaller but more frequent landslides.

Conclusions

Integrating sedimentological, physical and geotechnical data for quantitative submarine slope stability analysis offshore Uruguay and northern Argentina, a key finding of the present study is that distinct differences in primary lithological characteristics (such as grain size) controlled by bottom current velocities are associated with different slope stability conditions and modes of slope failures. This is reflected by the occurrence of infrequent landslides associated with retrogressive slope failures on open slopes characterized by fine-grained and potentially overpressured sedimentary successions. Sandy contouritic depositional systems, by contrast, are dominated by smaller but more frequent slope failures as well as gravity-driven downslope sediment transport within canyons. It is therefore concluded that the sedimentary and oceanographic settings represent key factors which precondition submarine landslide initiation and govern the mode of sediment mass transport along passive continental margins.

Furthermore, the slope stability calculations reveal that the continental slope is at present generally stable under static loading conditions, and that additional trigger mechanisms would be required to initiate failure. Where strong bottom currents locally influence the slope profile, oversteepening can occur and result in frequent small sediment remobilization events. On the more stable open slope, by contrast, the evaluation of static vs. seismic slope stability suggests that rare earthquakes may play a critical role in initiating slope failure along passive margins characterized by generally low seismicity. By implication, future submarine landslide studies and, for that matter, also slope stability hazard assessments for critical infrastructures offshore the east coast of South America should consider an integrated approach of combined slope stability and earthquake analysis, as proposed in this study for the Uruguayan and northern Argentinean margin.

Acknowledgements We thank the captain and crew of the R/V *Meteor* for their support during the M78/3 cruise. Matthias Lange is thanked for outstanding assistance with the geotechnical laboratory work. This study was funded through the DFG-Research Center/Cluster of Excellence "The Ocean in the Earth System", as well as the Chinese Scholarship Council (to F.A.), the Swiss National Science Foundation (grant 133481 to M.S.) and the German Research Foundation DFG (grant HA4317/4-1 to TH). We highly appreciate constructive comments by S. Lafuerza, an anonymous reviewer and the journal editors which greatly helped improving an initial version of this manuscript.

References

Ai F, Kuhlmann J, Huhn K, Strasser M, Kopf A (2014) Submarine slope stability assessment of the central Mediterranean continental margin: the Gela Basin. In: Krastel S, Behrmann J-H, Völker D, Stipp M, Berndt C, Urgeles R, Chaytor J, Huhn K, Strasser M, Harbitz CB (eds) Submarine mass movements and their consequences. Springer, Heidelberg, pp 225–236. doi:10.1007/978-3-319-00972-8_20

Assumpção M (1998) Seismicity and stresses in the Brazilian passive margin. Bull Seismol Soc Am 88:160–169

ASTM (2004a) Standard test methods for one-dimensional consolidation properties of soils using incremental loading. ASTM International, West Conshohocken, PA

ASTM (2004b) Standard test method for direct shear test of soils under consolidated drained conditions. ASTM International, West Conshohocken, PA

Baraza J, Ercilla G (1994) Geotechnical properties of near-surface sediments from the Northwestern Alboran Sea slope (SW Mediterranean): influence of texture and sedimentary processes. Mar Georesources Geotechnol 12:181–200. doi:10.1080/10641199409388261

Biscontin G, Pestana JM (2006) Factors affecting seismic response of submarine slopes. Nat Hazards Earth Syst Sci 6:97–107. doi:10.5194/nhess-6-97-2006

Blum P (1997) Physical properties handbook: a guide to the shipboard measurement of physical properties of deep-sea cores. ODP Tech Note 26. doi:10.2973/odp.tn.26.1997

Boyce RRE (1977) Deep Sea Drilling Project procedures for shear strength measurement of clayey sediment using modified Wykeham Farrance laboratory vane apparatus. Initial Reports DSDP, vol 36. US Government Printing Office, Washington, DC. doi:10.2973/dsdp.proc.36.app5.1977

Bozzano G, Violante RA, Cerredo ME (2011) Middle slope contourite deposits and associated sedimentary facies off NE Argentina. Geo-Mar Lett 31:495–507. doi:10.1007/s00367-011-0239-x

Bryn P, Berg K, Stoker MS, Haflidason H, Solheim A (2005) Contourites and their relevance for mass wasting along the Mid-Norwegian Margin. Mar Petrol Geol 22:85–96. doi:10.1016/j.marpetgeo.2004.10.012

Campbell KW, Bozorgnia Y (2008) NGA ground motion model for the geometric mean horizontal component of PGA, PGV, PGD and 5% damped linear elastic response spectra for periods ranging from 0.01 to 10 s. Earthquake Spectra 24:139–171. doi:10.1193/1.2857546

Casagrande A (1932) Research on the Atterberg limits of soils. Public Roads 13(8):121–136

Casagrande A (1936) The determination of the pre-consolidation load and its practical significance. In: Proc 1st Int Conf Soil Mechanics and Foundation Engineering, June 1936, Cambridge, MA. Harvard Printing Office, pp 60–64

Craig RF (2004) Craig's soil mechanics. CRC Press, Boca Raton, FL

Dugan B, Flemings PB (2002) Fluid flow and stability of the US continental slope offshore New Jersey from the Pleistocene to the present. Geofluids 2:137–146. doi:10.1046/j.1468-8123.2002.00032.x

Ewing M, Lonardi AG (1971) Sediment transport and distribution in the Argentine Basin. 5. Sedimentary structure of the Argentine margin, basin, and related provinces. Phys Chem Earth 8:123–251

Flemings PB, Long H, Dugan B, Germaine J, John CM, Behrmann JH, Sawyer D, Scientists IE (2008) Pore pressure penetrometers document high overpressure near the seafloor where multiple submarine landslides have occurred on the continental slope, offshore Louisiana, Gulf of Mexico. Earth Planet Sci Lett 269:309–325. doi:10.1016/j.epsl.2007.12.005

Franke D, Neben S, Ladage S, Schreckenberger B, Hinz K (2007) Margin segmentation and volcano-tectonic architecture along the volcanic margin off Argentina/Uruguay, South Atlantic. Mar Geol 244:46–67. doi:10.1016/j.margeo.2007.06.009

Garming JFL, Bleil U, Riedinger N (2005) Alteration of magnetic mineralogy at the sulfate–methane transition: analysis of sediments from the Argentine continental slope. Phys Earth Planet Interiors 151:290–308. doi:10.1016/j.pepi.2005.04.001

Giberto DA, Bremec CS, Acha EM, Mianzan H (2004) Large-scale spatial patterns of benthic assemblages in the SW Atlantic: the Río de la Plata estuary and adjacent shelf waters. Estuar Coastal Shelf Sci 61:1–13. doi:10.1016/j.ecss.2004.03.015

Gibson R (1958) The progress of consolidation in a clay layer increasing in thickness with time. Géotechnique 8(4):171–182

Hampton MA, Lee HJ, Locat J (1996) Submarine landslides. Rev Geophys 34:33–59. doi:10.1029/95RG03287

Harders R, Kutterolf S, Hensen C, Moerz T, Brueckmann W (2010) Tephra layers: a controlling factor on submarine translational sliding? Geochem Geophys Geosyst 11, Q05S23. doi:10.1029/2009GC002844

Henkel S, Strasser M, Schwenk T, Hanebuth TJJ, Hüsener J, Arnold GL, Winkelmann D, Formolo M, Tomasini J, Krastel S, Kasten S (2011) An interdisciplinary investigation of a recent submarine mass transport deposit at the continental margin off Uruguay. Geochem Geophys Geosyst 12, Q08009. doi:10.1029/2011GC003669

Hinz K, Neben S, Schreckenberger B, Roeser HA, Block M, Souza KG, Meyer H (1999) The Argentine continental margin north of 48°S: sedimentary successions, volcanic activity during breakup. Mar Petrol Geol 16:1–25. doi:10.1016/S0264-8172(98)00060-9

Huhn K, Kock I, Kopf A (2006) Comparative numerical and analogue shear box experiments and their implications for the mechanics along the failure plane of landslides. Norw J Geol 86:209–220

Hühnerbach V, Masson DG, partners of the COSTA-Project (2004) Landslides in the North Atlantic and its adjacent seas: an analysis of their morphology, setting and behaviour. Mar Geol 213:343–362. doi:10.1016/j.margeo.2004.10.013

Huppertz TJ (2011) Styles of continental margin sedimentation: comparing glaciated and non-glaciated slope systems using case studies on the southeast Canadian and northern Argentine and Uruguay continental slope. PhD thesis, FB5, University of Bremen, Bremen

Klaus A, Ledbetter MT (1988) Deep-sea sedimentary processes in the Argentine Basin revealed by high-resolution seismic records (3.5 kHz echograms). Deep Sea Res A Oceanogr Res Pap 35:899–917. doi:10.1016/0198-0149(88)90067-2

Krastel S, Wefer G, Hanebuth TJJ, Antobreh AA, Freudenthal T, Preu B, Schwenk T, Strasser M, Violante R, Winkelmann D (2011) Sediment dynamics and geohazards off Uruguay and the de la Plata River region (northern Argentina and Uruguay). Geo-Mar Lett 31:271–283. doi:10.1007/s00367-011-0232-4

Krastel S, Wefer G, cruise M78/3 scientific party (2012) Sediment transport off Uruguay and Argentina: from the shelf to the deep sea. Report and preliminary results of RV METEOR Cruise M78/3. Fachbereich Geowissenschaft Universität Bremen, Bremen

Krastel S, Lehr J, Winkelmann D, Schwenk T, Preu B, Strasser M, Wynn RB, Georgiopoulou A, Hanebuth TJJ (2014) Mass wasting along Atlantic continental margins: a comparison between NW-Africa and the de la Plata River region (northern Argentina and Uruguay). In: Krastel S, Behrmann J-H, Völker D, Stipp M, Berndt C, Urgeles R, Chaytor J, Huhn K, Strasser M, Harbitz CB (eds) Submarine mass movements and their consequences. Springer, Heidelberg, pp 459–469. doi:10.1007/978-3-319-00972-8_41

Kvalstad TJ, Nadim F, Kaynia AM, Mokkelbost KH, Bryn P (2005) Soil conditions and slope stability in the Ormen Lange area. Mar Petrol Geol 22:299–310. doi:10.1016/j.marpetgeo.2004.10.021

Lamb TW, Whitman RV (1969) Soil mechanics. Wiley, New York

Lee HJ, Chough SK, Jeong KS, Han SJ (1987) Geotechnical properties of sediment cores from the southeastern Yellow Sea: effects of depositional processes. Mar Geotechnol 7:37–52. doi:10.1080/10641198709388204

Lee H, Locat J, Dartnell P, Israel K, Florence W (1999) Regional variability of slope stability: application to the Eel margin, California. Mar Geol 154:305–321. doi:10.1016/S0025-3227(98)00120-0

Leynaud D, Mienert J, Nadim F (2004) Slope stability assessment of the Helland Hansen area offshore the mid-Norwegian margin. Mar Geol 213:457–480. doi:10.1016/j.margeo.2004.10.019

Leynaud D, Mienert J, Vanneste M (2009) Submarine mass movements on glaciated and non-glaciated European continental margins: a review of triggering mechanisms and preconditions to failure. Mar Petrol Geol 26:618–632. doi:10.1016/j.marpetgeo.2008.02.008

Locat J, Lee HJ (2002) Submarine landslides: advances and challenges. Can Geotech J 39:193–212. doi:10.1139/t01-089

Locat J, Lee H (2009) Submarine mass movements and their consequences: an overview. In: Sassa K, Canuti P (eds) Landslides - Disaster risk reduction. Springer, Heidelberg, pp 115–142

Lonardi AG, Ewing M (1971) Sediment transport and distribution in the Argentine Basin. 4. Bathymetry of the continental margin, Argentine Basin and other related provinces. Canyons and sources of sediments. Phys Chem Earth 8:79–121

Løseth TM (1999) Submarine massflow sedimentation: computer modelling and basin-fill stratigraphy. Lecture Notes in Earth Sciences, vol 82. Springer, New York

Lunne T, Berre T, Strandvik S (1997) Sample disturbance effects in soft low plastic Norwegian clay. In: Almeida M (ed) Proc 6th Int Symp Recent Developments in Soil and Pavement Mechanics, June 1997, Rio de Janeiro. A.A. Balkema, Rotterdam, pp 81–102

Masson DG, Harbitz CB, Wynn RB, Pedersen G, Løvholt F (2006) Submarine landslides: processes, triggers and hazard prediction. Philos Trans R Soc A Math Phys Eng Sci 364:2009–2039. doi:10.1098/rsta.2006.1810

Migeon S, Cattaneo A, Hassoun V, Larroque C, Corradi N, Fanucci F, Dano A, Mercier de Lepinay B, Sage F, Gorini C (2011) Morphology, distribution and origin of recent submarine landslides of the Ligurian Margin (North-western Mediterranean): some insights into geohazard assessment. Mar Geophys Res 32:225–243. doi:10.1007/s11001-011-9123-3

Morgenstern N (1967) Submarine slumping and the initiation of turbidity currents. In: Richards AF (ed) Marine geotechnique, proceedings. University of Illinois Press, pp 189–220

Mulder T, Tisot J-P, Cochonat P, Bourillet J-F (1994) Regional assessment of mass failure events in the Baie des Anges, Mediterranean Sea. Mar Geol 122(1/2):29–45

O'Grady DB, Syvitski JPM, Pratson LF, Sarg JF (2000) Categorizing the morphologic variability of siliciclastic passive continental margins. Geology 28:207–210

Piola AR, Matano RP (2001) Brazil and Falklands (Malvinas) currents. In: John HS (ed) Ocean currents: A derivative of the Encyclopedia of Ocean Sciences. Academic Press, Oxford, pp 35–43

Piola AR, Matano RP, Palma ED, Möller OO, Campos EJD (2005) The influence of the Plata River discharge on the western South Atlantic shelf. Geophys Res Lett 32, L01603. doi:10.1029/2004GL021638

Preu B, Schwenk T, Hernández-Molina FJ, Violante R, Paterlini M, Krastel S, Tomasini J, Spieß V (2012) Sedimentary growth pattern on the northern Argentine slope: the impact of North Atlantic Deep Water on southern hemisphere slope architecture. Mar Geol 329(331):113–125. doi:10.1016/j.margeo.2012.09.009

Preu B, Hernández-Molina FJ, Violante R, Piola AR, Paterlini CM, Schwenk T, Voigt I, Krastel S, Spiess V (2013) Morphosedimentary and hydrographic features of the northern Argentine margin: the interplay between erosive, depositional and gravitational processes and its conceptual implications. Deep Sea Res I Oceanogr Res Pap 75:157–174. doi:10.1016/j.dsr.2012.12.013

Puga-Bernabéu Á, Webster JM, Beaman RJ (2013) Potential collapse of the upper slope and tsunami generation on the Great Barrier Reef margin, north-eastern Australia. Nat Hazards 66:557–575. doi:10.1007/s11069-012-0502-0

Seed HB (1979) Considerations in the earthquake-resistant design of earth and rockfill dams. Géotechnique 29:215–263

Seed HB, Idriss IM (1971) Simplified procedure for evaluation soil liquefaction potential. J Soil Mechanics Foundations Division 97:1249–1273

Silva A (1974) Marine geomechanics: overview and projections. In: Inderbitzen A (ed) Deep-sea sediments. Springer, New York, pp 45–76

Sosa AB (1998) Sismicidad y sismotectónica en Uruguay. Física tierra 10:167–186

Stigall J, Dugan B (2010) Overpressure and earthquake initiated slope failure in the Ursa region, northern Gulf of Mexico. J Geophys Res Solid Earth 115, B04101. doi:10.1029/2009JB006848

Strasser M, Hilbe M, Anselmetti F (2011) Mapping basin-wide subaquatic slope failure susceptibility as a tool to assess regional seismic and tsunami hazards. Mar Geophys Res 32:331–347. doi:10.1007/s11001-010-9100-2

Sultan N, Cochonat P, Canals M, Cattaneo A, Dennielou B, Haflidason H, Laberg JS, Long D, Mienert J, Trincardi F, Urgeles R, Vorren TO, Wilson C (2004) Triggering mechanisms of slope instability processes and sediment failures on continental margins: a geotechnical approach. Mar Geol 213:291–321. doi:10.1016/j.margeo.2004.10.011

Sultan N, Gennaro VD, Puech A (2012) Mechanical behaviour of gas-charged marine plastic sediments. Géotechnique 62:751–766

ten Brink US, Lee HJ, Geist EL, Twichell DC (2009) Assessment of tsunami hazard to the U.S. East Coast using relationships between submarine landslides and earthquakes. Mar Geol 264:65–73. doi:10.1016/j.margeo.2008.05.011

Terzaghi K, Peck RB, Mesri G (1996) Soil mechanics in engineering practice. Wiley, New York

Urgeles R, Camerlenghi A (2013) Submarine landslides of the Mediterranean Sea: trigger mechanisms, dynamics, and frequency-magnitude distribution. J Geophys Res Earth Surface 118:2600–2618. doi:10.1002/2013JF002720

Voigt I, Henrich R, Preu BM, Piola AR, Hanebuth TJJ, Schwenk T, Chiessi CM (2013) A submarine canyon as a climate archive—interaction of the Antarctic Intermediate Water with the Mar del Plata Canyon (Southwest Atlantic). Mar Geol 341:46–57. doi:10.1016/j.margeo.2013.05.002

Wood DM (1985) Some fall-cone tests. Géotechnique 35:64–68